ACS APPLIED MATERIALS & INTERFACES

Research Article

www.acsami.org

Photocurrent Enhancement of BODIPY-Based Solution-Processed Small-Molecule Solar Cells by Dimerization via the Meso Position

Wenxu Liu,[§,‡] Ailing Tang,[§] Jianwei Chen,[†,§] Yishi Wu,[†,∥] Chuanlang Zhan,*[,§] and Jiannian Yao[§]

[†]Beijing National Laboratory of Molecular Science, [§]CAS Key Laboratory of Photochemistry, Institute of Chemistry, and [∥]State Key Laboratory for Structural Chemistry of Unstable and Stable Species, Chinese Academy of Sciences, Beijing 100190, P. R. China

[‡]Graduate School, Chinese Academy of Sciences, Beijing 100039, P. R. China

Supporting Information

ABSTRACT: Three 4,4-difluoro-4-bora-3a,4a-diaza-*s*-indancene (BODIPY)-based small molecule donors **H-T-BO**, **Br-T-BO**, and **DIMER** were synthesized and fully characterized. Although modification at the meso position has a subtle influence on the light-harvesting ability, energy levels, and phase sizes, it has a striking effect on the packing behavior in solid film as two-dimension grazing incidence X-ray diffraction (2D GIXRD) and X-ray diffraction (XRD) confirm. **Br-T-BO** exhibits better packing ordering than **H-T-BO** in pristine film, which is beneficial from reinforced intermolecular interaction from halogen atoms. However, when [6,6]-phenyl-C_{71}-butyric acid methyl ester ($PC_{71}BM$) is blended, no diffraction patterns corresponding to the monomeric donor can be seen from the XRD data and both **H-T-BO**- and **Br-T-BO**-based blend films give a slightly blue-shifting absorption peak with respect to their neat ones, both of which imply destruction of the crystalline structure. As for **DIMER**, the enhancement of the intermolecular interaction arises not only from the expansion of the backbone but the "steric pairing effect" brought on by its twisted structure. When blended with $PC_{71}BM$, the diffraction patterns of **DIMER** are, however, kept well and the absorption peak position remains unchanged, which indicates the ordered packing of **DIMER** is held well in blend film. In coincidence with the fact that packing ordering improves from **H-T-BO** to **Br-T-BO** and **DIMER** in pristine films and the ordered packing of **DIMER** even in blend film, **DIMER**-based devices show the highest and most balanced hole/electron mobility of $1.16 \times 10^{-3}/0.90 \times 10^{-3}$ cm^2 V^{-1} $s^{-1}$with respect to **Br-T-BO** ($4.71 \times 10^{-4}/2.09 \times 10^{-4}$ cm^2 V^{-1} s^{-1}) and **H-T-BO** ($4.27 \times 10^{-5}/1.00 \times 10^{-5}$ cm^2 V^{-1} s^{-1}) based ones. The short-circuit current density of the three molecule-based cells follows the same trend from **H-T-BO** (6.80) to **Br-T-BO** (7.62) and then to **DIMER** (11.28 mA cm^{-2}). Finally, the **H-T-BO**-, **Br-T-BO**-, and **DIMER**-based optimal device exhibits a power conversion efficiency of 1.56%, 1.96%, and 3.13%, respectively.

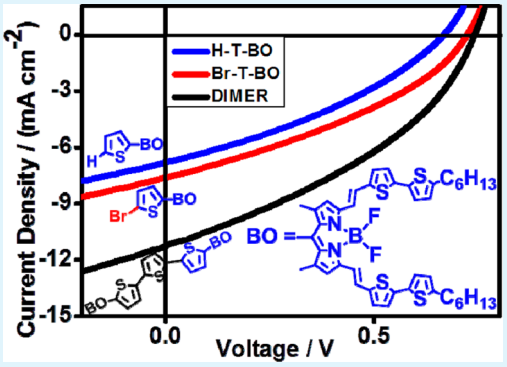

KEYWORDS: *BODIPY, small molecule, donor, solution-processed, organic solar cell*

INTRODUCTION

During recent decades, organic solar cells (OSCs) have drawn much attention for some properties they possess, such as being lightweight and low cost and having flexible device applications.[1−4] To date, a power conversion efficiency (PCE) over 9% has been achieved in single-junction polymer solar cells (PSCs) with continuous endeavor.[5−7] Meanwhile, since small molecule donors bear some unique advantages, including well-defined structures and molecular weight as well as easy purification, solution-processed small molecule solar cells (SMSCs) are investigated as competitive alternatives to their polymer counterparts.[8−12] In the past few years, the PCE of the state-of-the-art SMSCs has reached over 8%, however, only from two types of small molecules unfortunately.[13,14] In order to catch up with the pace of PSCs, great efforts should be made to develop materials with new structures as well as to understand the relationship between the molecular structure and the performance.[15−19]

Derivatives of 4,4-difluoro-4-bora-3a,4a-diaza-*s*-indancene (BODIPY) are known as "porphyin's little sister".[20] They show large molar extinction coefficients (ε) with ε_{max} usually larger than 8×10^4 M^{-1} cm^{-1} together with excellent chemical stability to withstand a series of chemical transformations.[21−27] However, the BODIPY core usually gives a sharp absorption band with a maximum absorption wavelength (λ_{max}) at 500 nm and a band edge (λ_{edge}) less than 550 nm,[28] which impedes full use of the solar photons, since ca. 50% of photons in the solar spectrum have energies corresponding to a wavelength of 600−1000 nm.[29] How to red shift and broaden the absorption band is a bottleneck to achieve a higher PCE for BODIPY-based donor materials. To break through the bottleneck, one effective way is to functionalize the α and β positions of the BODIPY core to extend the conjugation. After that, the BODIPY dyes

Received: September 24, 2014
Accepted: November 26, 2014
Published: November 26, 2014

dx.doi.org/10.1021/am506585u | *ACS Appl. Mater. Interfaces* 2014, 6, 22496−22505

always exhibit broader absorption with λ_{max} > 600 nm,[28,30,31] which means that more solar photons can be captured. Consequently, a higher short-circuit current density (J_{sc}) and PCE can be anticipated.[32−37]

Besides a broad absorption band with a large ε, it is of importance to guarantee well-ordered packing in a solid film to achieve a high hole/electron mobility and thus the J_{sc}. It has been proved that reinforcing the intermolecular interaction is efficacious in the enhancement of the packing ordering in a solid.[38,39] As for BODIPY-based system, Ziessel etc., for example, reported that the halogen interaction between the I atom at the meso position and one of the F atoms of the neighboring molecule can strengthen the intermolecular interaction, thus facilitating the molecules to pack in a well-organized way, which is linked with the improvement of both the charge carriers mobility and the J_{sc}.[35]

In this article we present a new way to reinforce the intermolecular interaction and packing ordering. We find that dimerization of two BODIPY units through the meso position proves to be an effective approach to promoting the mobility and J_{sc}. To investigate the origin of the enhancement of the J_{sc}, we also synthesized two relevant monomers (**H-T-BO** and **Br-T-BO**, Scheme 1). Our results imply that the enhancement of the intermolecular interaction and the ordered packing make contributions to boosting the hole/electron mobility and the J_{sc}. **Br-T-BO** packs more orderly than **H-T-BO** in neat film, thanks to the intermolecular interaction from the halogen bond. On the other hand, **DIMER** shows order and tight packing both in pure film and in a blended one with [6,6]-phenyl-C_{71}-butyric acid methyl ester ($PC_{71}BM$), which attributes to the enhancement of intermolecular interaction owing to its enlarged and twisted structure. Consistently, a slight increase of the hole/electron mobility and J_{sc} from **H-T-BO**- to **Br-T-BO**-based cell is observed, while a significant enhancement further to **DIMER** is obtained.

Scheme 1. Structure of H-T-BO, Br-T-BO, and DIMER

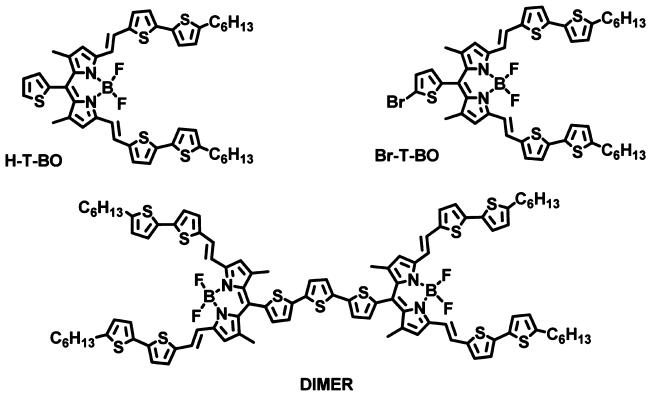

RESULTS AND DISCUSSION

Synthesis and Characterization. Scheme 2 outlines the synthetic routes of **H-T-BO**, **Br-T-BO**, and **DIMER**. Condensation of 2,4-dimethylpyrrole with the corresponding aromatic aldehydes (2-thiophenecarboxaldehyde and 5-bromo-2-thiophenecarboxaldehyde) followed by adding 2,3-dichloro-5,6-dicyano-1,4-benzoquinone (DDQ), $(i\text{-Pr})_2$EtN, and BF_3-Et_2O gave the desired products (**2**, yield 35%; **3**, yield 36%). The following condensation with aldehyde (**1**) gave **H-T-BO** and **Br-T-BO** in moderate yield (40% for **H-T-BO** and 38% for **Br-T-BO**). Finally, Stille coupling between **Br-T-BO** and 2,5-bis(tributylstannyl)thiophene produced **DIMER** with a yield of 40%. All of the three donors exhibit good solubility in common solvents, such as dichloromethane (DCM), chloroform, toluene, chlorobenzene, and 1,2-dichlorobenzene (*o*-DCB). All three donors were fully characterized by ^{1}H NMR, ^{13}C NMR, MALDI-TOF MS, and elemental analysis successfully (Experimental Section).

Thermogravimetric (TGA) curves provide useful information about the thermostability of the three donors. Judging from the curves (Figure S1, Supporting Information), one can find that the temperatures with 5% weight loss of **H-T-BO**, **Br-T-BO**, and **DIMER** are 338.8, 261.3, and 342.0 °C, respectively. Clearly, introduction of the Br atom has a detrimental effect on the thermostability of the molecule.

Scheme 2. Synthesis of H-T-BO, Br-T-BO, and DIMER[a]

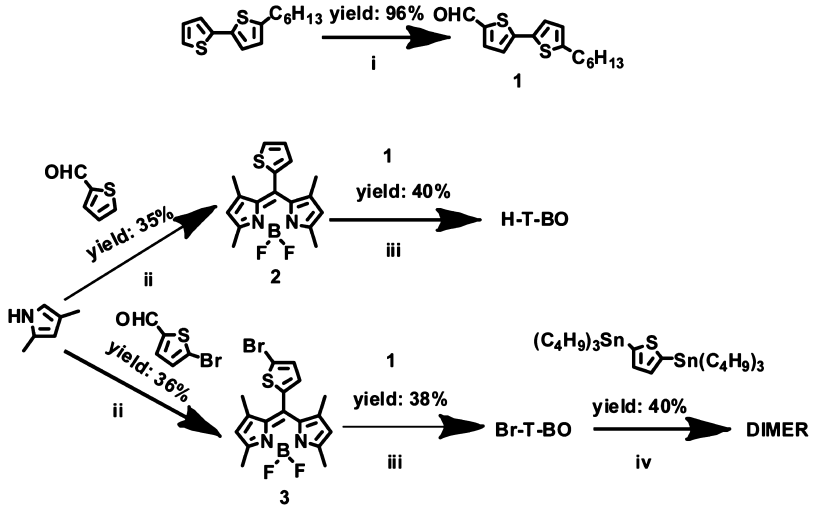

[a](i) *n*-BuLi, DMF, THF, yield 96%; (ii) TFA, DDQ, $(i\text{-Pr})_2$EtN, BF_3-Et_2O, N_2, CH_2Cl_2, yield 35% for compound **2**, 36% for compound **3**; (iii) **1**, piperidine, CH_3COOH, molecule sieves, N_2, 90 °C, toluene, yield 40% for **H-T-BO** and 38% for **Br-T-BO**; (iv) 2,5-bis(tributylstannyl)thiophene, $Pd(PPh_3)_4$, N_2, 90 °C, toluene, yield 40%.

dx.doi.org/10.1021/am506585u | ACS Appl. Mater. Interfaces 2014, 6, 22496−22505

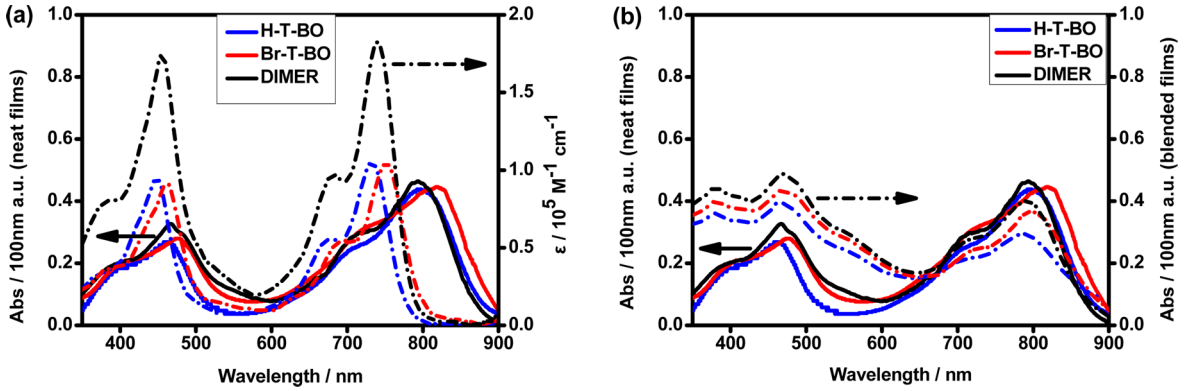

Figure 1. UV−vis absorption spectra of the three donors from (a) the dilute DCM solution and the neat films and (b) the blend films (1:2 for **H-T-BO**:$PC_{71}BM$ and 1:2.5 for **Br-T-BO**:$PC_{71}BM$ and **DIMER**:$PC_{71}BM$, w/w). In b the absorption spectra from the neat films are also displayed for comparison.

Optoelectronic Properties. Figure 1a depicts the UV−vis absorption spectra of the three BODIPY-based donors in dilute DCM solution and in thin films. All of the molecules show two broad absorption bands from 350 to 500 nm and from 650 to 800 nm in solution with two peaks at about 450 and 740 nm. The former absorption is due to the styryl residues, while the latter one with an apparent shoulder arises from the S_0 to the S_1 transition.[35,37] The optimal geometry of **DIMER** calculated by density function theory (DFT) reveals that **DIMER** exhibits a highly twisted backbone with a dihedral angle of about 89° between the terthienyl plane and the dipyrromethene plane (Figure 2). The twisted structure is in accordance with the optical phenomenon that the ε_{max} of **DIMER** is almost twice that of the monomer.[26] Compared with the spectrum in solution, that of the pristine film from the same donor is significantly red shifted and broadened, which indicates that the molecules form aggregates in the solid. As shown in Figure 1b and Table 1, the λ_{max} of **H-T-BO** and **Br-T-BO** exhibits a hypochromic shift when blended with $PC_{71}BM$ while the λ_{max} of **DIMER** remains unchanged with respect to the corresponding pristine film. The spectral phenomenon implies that the aggregates may be disrupted to a degree when **H-T-BO** and **Br-T-BO** are blended with $PC_{71}BM$, while it can be retained in the **DIMER**:$PC_{71}BM$ blend.[40] Given that the shift of λ_{max} is less than 20 nm and the three BODIPY-based donors present almost the same onset of the absorption band in blend films, modification at the meso position has no perceptible effect on the light harvesting in this study.

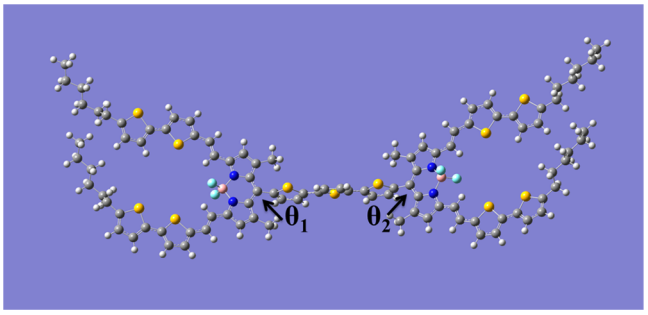

Figure 2. Optimal geometry of **DIMER** calculated by DFT. Dihedral angles between one BODIPY plane and the terthienyl plane are defined as θ_1 (θ_1 = 88.6°) and θ_2 (θ_2 = 89.4°), respectively.

The electrochemical properties of the three donors were investigated using cyclic voltammetry (CV). Table 1 summarizes the electrochemical data. The onset of the oxidation potentials of **H-T-BO**, **Br-T-BO**, and **DIMER** are estimated to be 0.62, 0.66, and 0.66 V, while the onset of the reduction potentials are at −0.76, −0.66, and −0.67 V, respectively (Figure 3a). On the basis of on the empirical equation ($E_{HOMO} = -e(E_{ox,onset} + 4.4)$; $E_{LUMO} = -e(E_{red,onset} + 4.4)$)[41] the corresponding HOMO/LUMO energy levels of **H-T-BO**, **Br-T-BO**, and **DIMER** are −5.02/−3.64, −5.06/−3.74, and −5.06/−3.73 eV (Figure 3b), respectively. According to the formula $E_g = E_{LUMO} - E_{HOMO}$, the electrochemical band gaps of **H-T-BO**, **Br-T-BO**, and **DIMER** are calculated to be 1.38, 1.32, and 1.33 eV, respectively. $PC_{71}BM$ has HOMO and LUMO energy levels of −5.87 and −3.91 eV. Compared with the energy levels of $PC_{71}BM$, all three molecules are potential donor materials.

Table 1. Summary of the Optoelectronic Properties of the Three Donors

		λ_{max}[a]/nm		λ_{edge}[d]/nm					
molecule	solution	film$_p$[b]	film$_b$[c]	solution	film$_p$[e]	E_g^{opt}[f], eV	HOMO, eV	LUMO, eV	E_g^{cv}[g], eV
H-T-BO	448	463	462	775	885	1.40	−5.02	−3.64	1.38
	733	804	788						
Br-T-BO	460	476	468	800	900	1.38	−5.06	−3.74	1.32
	752	811	794						
DIMER	456	467	468	780	880	1.41	−5.06	−3.73	1.33
	741	794	794						

[a]Absorption maximum. [b]λ_{max} in pristine (p) films. [c]λ_{max} in blend (b) films. [d]Onset of the absorption. [e]λ_{edge} from pristine films. [f]Optical band gap, $E_g^{opt} = 1240/\lambda_{edge}$. [g]Electrochemical band gap, $E_g^{cv} = E_{LUMO} - E_{HOMO}$.

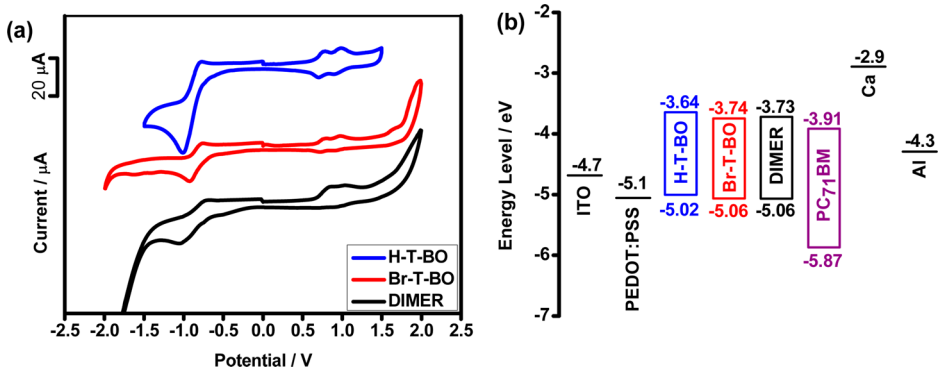

Figure 3. (a) Cyclic voltammograms of the three donors in DCM with 0.1 M Bu_4NPF_6. Scan rate was 100 mV s^{-1}, Ag/AgCl was used as reference electrode. (b) Energy level diagram of the three donors, $PC_{71}BM$, as well as other essential components for the normal cell structure.

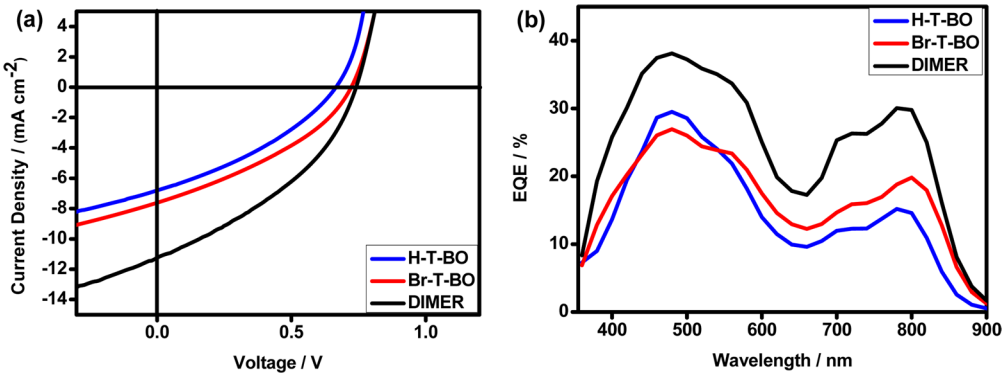

Figure 4. (a) *J*–*V* characteristics and (b) EQE curves of **H-T-BO**-, **Br-T-BO**-, and **DIMER**-based cells under the optimal D:A weight ratio.

Table 2. Photovoltaic Parameters of the SMSCs under Optimal D:A Weight Ratio

donor:acceptor	D:A (w:w)	J_{sc}[a] (mA cm^{-2})	V_{oc}[a] (V)	FF[a] (%)	PCE[a] (%)
H-T-BO:$PC_{71}BM$	1:2	6.80 (±0.16)	0.67 (±0.01)	34.3 (±1.2)	1.56 (±0.08)
Br-T-BO:$PC_{71}BM$	1:2.5	7.62 (±0.14)	0.72 (±0.01)	35.7 (±1.3)	1.96 (±0.10)
DIMER:$PC_{71}BM$	1:2.5	11.28 (±0.28)	0.74 (±0.01)	37.5 (±0.8)	3.13 (±0.13)

[a]Average value from 10 devices with the standard deviation in parentheses.

Photovoltaic Performance. In order to investigate the photovoltaic performance of the three donors, cell devices based on the conventional device structure of ITO/poly(3,4-ethylene-dioxythiophene) (PEDOT):poly(styrenesulfonate) (PSS)/active layers/Ca/Al were fabricated. Details of the fabrication of the devices are given in the Experimental Section. The weight ratio of the donor and acceptor was optimized for all three donors, and Table S1, Supporting Information, gives the corresponding results. The optimal donor:acceptor (D:A) weight ratio for **H-T-BO**:$PC_{71}BM$, **Br-T-BO**:$PC_{71}BM$, and **DIMER**:$PC_{71}BM$ is 1:2, 1:2.5, and 1:2.5, respectively. Figure 4a shows the current density–voltage (*J*–*V*) curves of the best cells from the three donors under the optimal D:A weight ratio. Table 2 lists the corresponding cell parameters.

From **H-T-BO** to **Br-T-BO** and then to **DIMER**, J_{sc} increases from 6.80 to 7.62 and then to 11.28 mA cm^{-2} sharply. Unfortunately, the fill factor (FF) grows very little from **H-T-BO** (0.343) to **Br-T-BO** (0.357) to **DIMER** (0.375). The low FF is always seen from the BODIPY-based solar cells.[33] As is known, the open-circuit voltage (V_{oc}) has a close relationship with the difference between the HOMO energy of the donor and the LUMO energy of the acceptor.[42−44] It is reasonable that **H-T-BO**:$PC_{71}BM$ blend film presents the lowest V_{oc} (0.67 V) because of the highest lying HOMO among the three, while the V_{oc} values of the other two donors are almost the same (0.72 V for **Br-T-BO** and 0.74 V for **DIMER**).

In order to validate the accuracy of the photovoltaic measurements, external quantum efficiency (EQE) measurements were conducted on the best cells. The EQE curves are shown in Figure 4b. Obviously, the EQE spectra from the three donors share a similar shape with their corresponding absorption spectra of the blend films. One can also see that all of the EQE curves cover a wide range of the optical spectrum (from 350 to 900 nm). The integrated current density (*J*) can be calculated by the following equation $J = \lambda P_{in}EQE/1240$, where P_{in} is the illumination intensity and λ is the wavelength of the monochromatic incident light.[45] The current density is calculated to be 6.50, 7.48, and 11.06 mA cm^{-2} for **H-T-BO**, **Br-T-BO**, and **DIMER**, respectively. These values match well with the J_{sc} data received from the best cells.

Taking the cell parameters into consideration, one can find that the enhancement of J_{sc} contributes to the improvement of the PCE with the blend donor changing from **H-T-BO** to **Br-T-BO** and then to **DIMER**. Since the shape and intensity of the absorption spectra of the active layers are almost the same, we

speculate that the enhancement of J_{sc} could have a relationship with the film morphology in a solid.

Film Morphology. Transmission electron microscopy (TEM) images were recorded to understand the nanoscale morphologies of the blend films. It can be seen from Figure 5

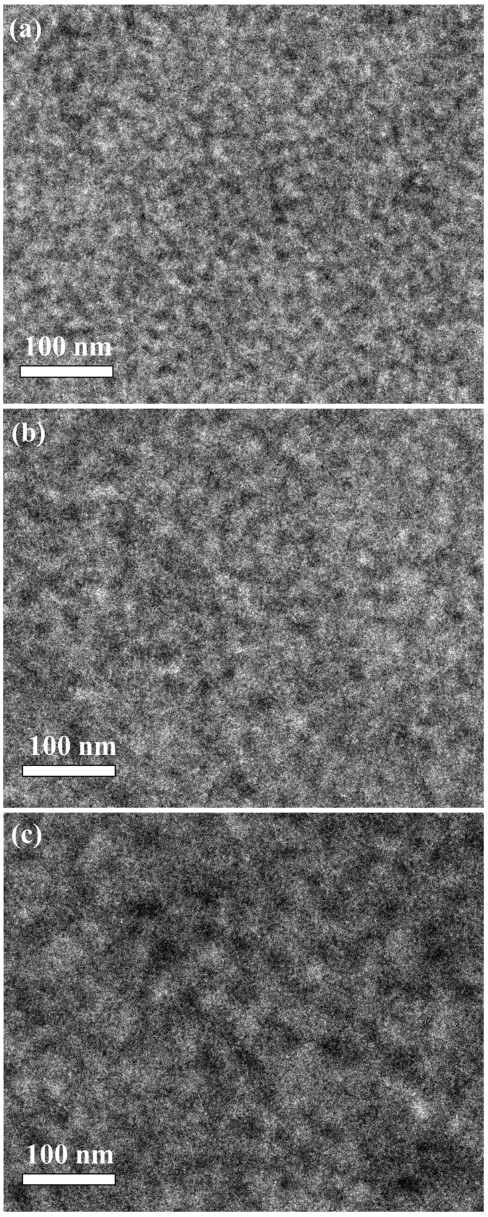

Figure 5. TEM images of (a) **H-T-BO**:$PC_{71}BM$, (b) **Br-T-BO**:$PC_{71}BM$, and (c) **DIMER**:$PC_{71}BM$ blend films.

that the nanoscale interpenetrating network forms in all blends and that the phase size is estimated to be 15−20, 20−25, and 30−35 nm for films of **H-T-BO**:$PC_{71}BM$, **Br-T-BO**:$PC_{71}BM$, and **DIMER**:$PC_{71}BM$, respectively. All sizes are comparable to the exciton diffusion length, typically 5−20 nm.[46]

Molecular Packing in Solid Films. Grazing-incidence X-ray diffraction (2D GIXRD) was applied to get a better understanding of the crystalline behavior of the three donors in the solid state with and without $PC_{71}BM$. Figure 6a−c shows 2D GIXRD images of the three neat films, and Figure S2, Supporting Information, is their linecut profiles along the out-of-plane and in-plane directions, respectively. The conspicuous signals in Figure 6a−c reveal the well-ordered crystalline structures in neat films. Specifically, each donor exhibits a strong (100) reflection peak along the q_z direction, with a q_z value of 0.244, 0.294, and 0.283 $Å^{-1}$ for **H-T-BO**, **Br-T-BO**, and **DIMER**, respectively. On the basis of the relationship between q and d spacing, $d = 2\pi/q$, the "lamellar" spacing can be determined as 25.8, 21.4, and 22.2 Å, respectively. As clearly seen from Figure 6b and 6c and from the out-of-plane linecut profiles (Figure S2, Supporting Information), higher order up to forth and even fifth diffractions can be clearly seen from the **Br-T-BO** and **DIMER** pure films, while only the second-order reflection is detected from the **H-T-BO** neat one. Clearly, **Br-T-BO** tends to pack more orderly and tightly than **H-T-BO** in neat films, and **DIMER** forms even more ordered packing because **DIMER** gives stronger higher order diffractions and, particularly, shows a clear arch shape of the (010) diffraction in the 2D GIXRD image (Figure 6c) with q = 1.82 $Å^{-1}$, which corresponds to a $\pi-\pi$ stacking distance of 3.45 Å. The appearance of the $\pi-\pi$ stacking diffraction pattern indicates even more ordered packing of the dimeric backbones in the film.

When the donor is blended with $PC_{71}BM$, all of the diffractions, even those corresponding to the strong (100) and (200) patterns, are not detected from the **H-T-BO**:$PC_{71}BM$ and **Br-T-BO**:$PC_{71}BM$ blend films, along neither the out-of-plane nor the in-plane direction (Figure 6d and 6e as well as Figures S2a and S2b, Supporting Information). On the contrary, from the **DIMER**:$PC_{71}BM$ blend, all of the (100), (200), (300), (400), and (500) as well as (010) (Figures 6f and S2c, Supporting Information) diffractions are clearly seen at their corresponding q values. That contrast between the neat and the blend films strongly indicates that packing ordering is held when **DIMER** is combined with $PC_{71}BM$, while it is disrupted when **H-T-BO** or **Br-T-BO** is used instead. The results are further confirmed by the XRD tests (Figure S3, Supporting Information), in which all of the diffraction peaks observed from the **H-T-BO** or **Br-T-BO** neat films disappear after they are blended with $PC_{71}BM$, whereas the diffraction patterns are well kept in the blend from **DIMER**.

Introduction of the Br atom at the meso position helps **Br-T-BO** stack in a more ordered way than **H-T-BO**, likely owing to the intermolecular interaction between the Br atom and the F atom, as observed previously from the iodo derivatives of BODIPY.[35] From monomer to dimer, the enlarged molecular backbone favors the ordered packing of **DIMER** in the solid. Moreover, the highly twisted structure of **DIMER** could provide the so-called "steric-pairing effect", which has been observed in other dimeric systems, such as perylene diimide (PDI).[47] This effect is also expected to direct the ordered packing of **DIMER** in the solid state. Therefore, the enlarged structure as well as the twisted conformation facilitates the **DIMER** molecules to form ordered packing not only in neat films but also in blend films with $PC_{71}BM$.

Hole/Electron Mobility. As the transport property of the charge carriers in blend films is of critical importance to the photovoltaic performance, hole-only devices with the structure ITO/PEDOT:PSS/small molecule donor:$PC_{71}BM$/Au were fabricated to characterize the hole mobility of the active layers, while electron-only devices with the configuration ITO/titanium (diisopropoxide) bis(2,4-pentanedionate) (TIPD)/small molecule donor:$PC_{71}BM$/Al were prepared to measure the electron mobility.[48−50] Also, the layers were prepared under the optimal conditions of the cell devices mentioned above.

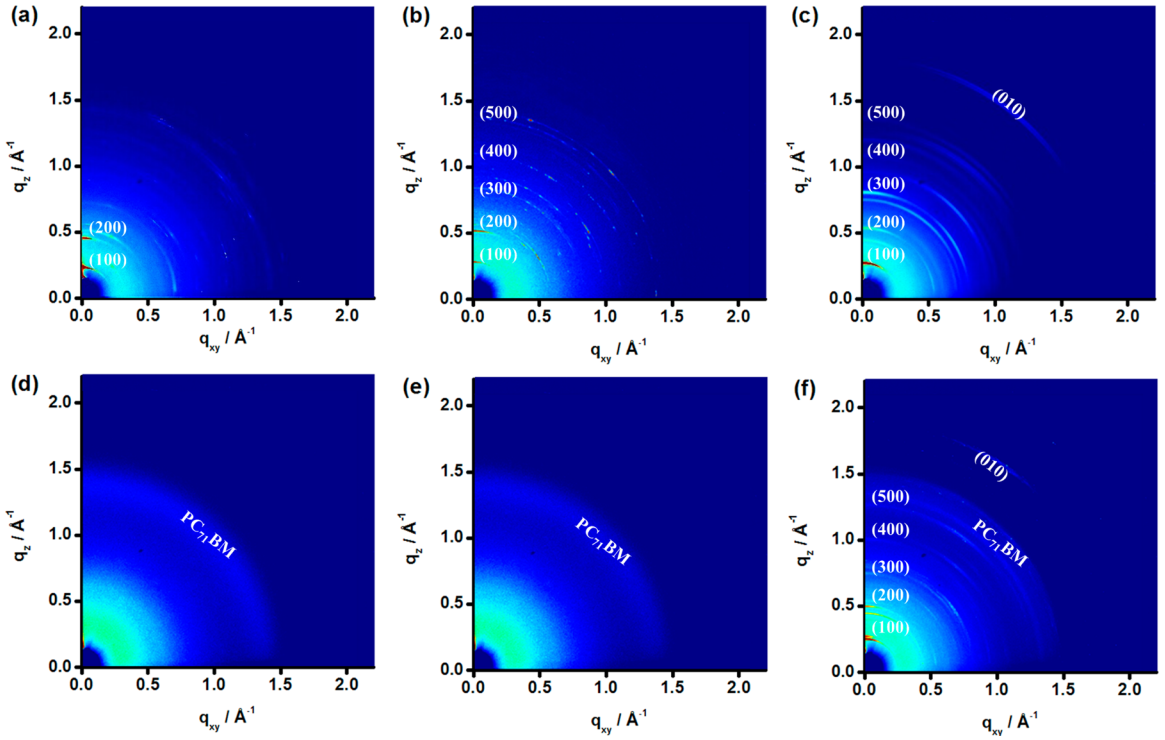

Figure 6. 2D GIXRD images of the three donors in neat (a–c) and blend films with $PC_{71}BM$ (d–f): (a) **H-T-BO**, (b) **Br-T-BO**, (c) **DIMER**, (d) **H-T-BO**:$PC_{71}BM$, (e) **Br-T-BO**:$PC_{71}BM$, and (f) **DIMER**:$PC_{71}BM$.

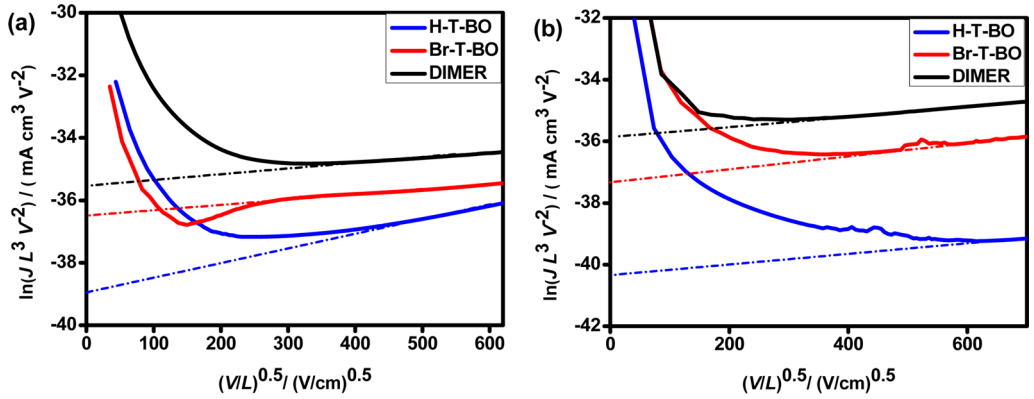

Figure 7. Plots of $\ln(JL^3/V^2)$ versus $(V/L)^{0.5}$ from the hole-only (a) and electron-only (b) devices.

Figure 7a and 7b shows the plots of $\ln(JL^3V^2)$ versus $(V/L)^{0.5}$ from the hole-only and electron-only devices. Both the hole and the electron mobility can be deduced directly from the intercept value $\ln(9\varepsilon\varepsilon_0\mu/8)$. The hole/electron mobility of the **H-T-BO**:$PC_{71}BM$, **Br-T-BO**:$PC_{71}BM$, and **DIMER**:$PC_{71}BM$ blend is estimated to be $4.27 \times 10^{-5}/1.00 \times 10^{-5}$, $4.71 \times 10^{-4}/2.09 \times 10^{-4}$, and $1.16 \times 10^{-3}/0.90 \times 10^{-3}$ $cm^2\ V^{-1}\ s^{-1}$, respectively. The hole and electron mobility both obey the sequence of **DIMER** > **Br-T-BO** > **H-T-BO**, which is a correlation with the sequence of J_{sc}. Meanwhile, the **DIMER**-based devices present the most balanced hole and electron mobility with respect to the monomers. In all, it becomes clear that the molecular ordering plays a role in the enhancement of the mobility and then the J_{sc} of BODIPY-based devices. Additionally, the charge dissociation at the donor–acceptor interfaces has a close relationship with generation of the charge carriers and may be another role in the boosting of J_{sc}, while we need more data to understand this.

CONCLUSIONS

Three new BODIPY-based solution-processable small molecule donors, **H-T-BO**, **Br-T-BO**, and **DIMER**, were designed and synthesized successfully. We find that **Br-T-BO** tends to pack in a more ordered way than **H-T-BO** in pristine film, which might benefit from the intermolecular interaction from the halogen bond. However, when $PC_{71}BM$ is blended, the packing ordering from the two monomers is devastated. In contrast, **DIMER** forms an even more ordered packing than **Br-T-BO** in pure film, and more interestingly, the packing ordering can be held well in blend films with $PC_{71}BM$. The enlarged conjugation and twisted structure of **DIMER** contributes to the enhancement of the intermolecular interaction which is conductive to the well-ordered packing even in blend films. The enhancement of the packing is in accord with the values of hole/electron mobility: **DIMER**-based device gives the highest and the most balanced hole/electron mobility ($4.27 \times 10^{-5}/1.00 \times 10^{-5}$ $cm^2\ V^{-1}\ s^{-1}$ for **H-T-BO**, $4.71 \times 10^{-4}/2.09 \times 10^{-4}$

dx.doi.org/10.1021/am506585u | ACS Appl. Mater. Interfaces 2014, 6, 22496–22505

$cm^2\ V^{-1}\ s^{-1}$ for **Br-T-BO**, and $1.16 \times 10^{-3}/0.90 \times 10^{-3}\ cm^2\ V^{-1}\ s^{-1}$ for **DIMER**) among the three. The J_{sc} values of the three donor-based devices share the same sequence with the charge carrier mobility: **H-T-BO** (6.80 mA cm^{-2}) < **Br-T-BO** (7.62 mA cm^{-2}) < **DIMER** (11.28 mA cm^{-2}). Since the great enhancement of the J_{sc}, the **DIMER**-based system possesses the highest PCE (1.56% **H-T-BO**, 1.96% for **Br-T-BO**, and 3.13% for **DIMER**). Whereas the modification at the meso position has a significant effect on the intermolecular interaction and packing ordering in the solid state in this study, three molecules appear to show comparable absorption spectra in blend films, energy levels, and phase sizes. Therefore, it is clear that the enhancement of the intermolecular interaction from **H-T-BO** to **Br-T-BO** to **DIMER** has a clear contribution to the improvement of the mobilities and therefore the J_{sc} and PCE. Our results demonstrate that dimerization via the meso position is an effective way to improve the J_{sc} of BODIPY-based SMSCs without bringing on a negative effect on the thermal stability with respect to introduction of the halogen atom.

EXPERIMENTAL SECTION

1. Instruments for Measurements and Characterization. ^1H and ^{13}C NMR spectra were obtained in chloroform-*d* ($CDCl_3$) with tetramethylsilane (TMS, δ = 0 ppm) as internal standard on a Bruker AVANCE 300 MHz or Bruker AVANCE 400 MHz. Mass spectra (MALDI-TOF-MS) were determined on a Bruker BIFLEX III mass spectrometer. Elemental analysis was performed on a flash EA1112 analyzer. Thermogravimetric analysis (TGA) was conducted on a diamond TG/DTA at a heating rate of 10 °C/min under N_2 flow. UV−vis absorption spectra were measured on a Shimadzu UV-2600 absorption spectrometer. Cycle voltammetry (CV) was measured on a computer-controlled Zennium electrochemical workstation at a scan rate of 100 mV/s. A glassy carbon electrode, a Pt wire, and a Ag/AgCl electrode were used as the working, counter, and reference electrodes, respectively. Samples were dissolved in degassed anhydrous dichloromethane with 0.1 M tetra-*n*-butylammonium hexafluorophosphate (Bu_4NPF_6) as the electrolyte. TEM tests were conducted on a JEM-2011F operated at 200 kV. Samples were prepared by transferring the solar cell active films to the 200 mesh copper grids. XRD data were recorded by a Rigaku D/max-2500 diffractometer operated at 40 kV voltage and 200 mA current with Cu Kα radiation. GIXRD data were recorded at 1W1A, Beijing Synchrotron Radiation Facility (BSRF, 1W1A). Samples were prepared by being drop cast in the solution in *o*-DCB on silica slides for pristine films, and blended films were fabricated by following the same procedure in fabricating the best cell devices except that silica slides were used. Density functional theory (DFT) computation was performed to optimize the conformation of **DIMER** by the Gaussian 03 program at the B3LYP/6-31G(d,p) level.

2. Fabrication of Organic Solar Cells and Hole/Electron Mobility Devices. Traditional architectures of organic solar cells:ITO/PEDOT:PSS/small molecule donor:$PC_{71}BM$/Ca/Al were fabricated. The indium tin oxide (ITO) glasses were cleaned with detergent, deionized water, acetone, and isopropanol and then treated in a Novascan PSD-ultraviolet-ozone chamber for 1 h before use. Afterward, a layer of 30 nm poly(3,4-ethylene-dioxythiophene):poly-(styrenesulfonate) (PEDOT:PSS, Baytron P VP AI 4083, Germany) was spin coated onto the surface of ITO glasses. After baking at 150 °C for 15 min in the air, the glasses were transferred into a glovebox. Then the *o*-DCB solution of small molecule/$PC_{71}BM$ with a total solid concentration of 40 mg mL^{-1} was spun cast carefully to form a photosensitive layer (ca. 110 nm). Finally, the Ca/Al cathode (ca. 20 nm/80 nm) was deposited by vacuum deposition onto the photosensitive layer. The effective area was 6 mm^2. The current density−voltage (J−V) measurement of the devices was measured using a computer-controlled Keithley 2400 Source Measure Unit in nitrogen atmosphere under white light illumination of simulated AM 1.5 G, 100 mW/cm^2 using a xenon-lamp-based solar simulator (AAA grade, XES-70S1). EQE measurements were measured using a 250 W Quartz Tungsten Halogen (Oriel) fitted with a monochromator (Cornerstone (CS130) 1/8m) as a monochromatic light source.

Devices with the configuration ITO/PEDOT:PSS/small molecule donor:$PC_{71}BM$/Au were fabricated to measure the hole mobility of the small molecules. In order to avoid penetration of Au atoms into the active layers, the Au layer was deposited at a speed of 0.1 Å/s. An electron-only device with the architecture of ITO/TIPD/small molecule donor:$PC_{71}BM$/Al was constructed to measure the electron mobility. Specifically, the TIPD layer was prepared by spin casting (3000 rpm, 35 s) the TIPD isopropanol solution with a concentration of 3.5 wt % and annealed at 150 °C for 10 min to convert TIPD into TOPD.[50] For both the hole-only and the electron-only devices, the active layer was spin coated under the same condition as preparation of the best organic solar cells and the current density−voltage measurement was also conducted on a Keithley 2400 Source Measure Unit. The charge carrier mobility was calculated according to the Mott−Gurney equation as follows: $\ln(JL^3V^2) = 0.89(1/E_0)^{0.5}(V/L)^{0.5} + \ln(9\varepsilon\varepsilon_0\mu/8)$, where ε is the dielectric constant of the blended film (here $\varepsilon \approx 3$), ε_0 is the permittivity of the vacuum (8.85419×10^{-12} F m^{-1}), μ_h is the zero-field mobility, E_0 is the characteristic field, J is the current density, L is the thickness of the films, and $V = V_{appl} - V_{bi}$ (here V_{appl} is the applied voltage to the device, V_{bi} is the build-in voltage which is caused by the difference of the work function between the two electrodes).

3. Materials and Synthetic Procedures. All of the starting materials and solvents were purchased from Sigma-Aldrich, Acros, or Alfa Aesar and used without further purification. Tetrahydrofuran (THF) and toluene were distilled from sodium benzophenone ketyl under the protection of N_2 before use.

Synthesis of Compound ***1***. 5-Hexyl-2,2′-bithiophene (300 mg, 1.2 mmol) and 10 mL of anhydrous THF were added into a dry Schlenk tube under a nitrogen atmosphere. Then the system was cooled to −78 °C, and *n*-BuLi (0.8 mL, 2 mmol, 2.5 M in hexanes) was added dropwise by a syringe. Afterward, the tube was warmed to room temperature gradually and stirred for 1 h; then anhydrous DMF (0.12 mL, 1.5 mmol) was added slowly and the reaction mixture was allowed to stir for another 2 h. After the reaction was completed, 30 mL of water was added to the mixture, which was extracted with CH_2Cl_2 three times. The organic layers were collected and dried over Na_2SO_4, and the solvent was evaporated under vacuum. The crude product was purified by column chromatography (eluent CH_2Cl_2/petroleum = 2/1) to afford a yellow solid as product (320 mg, yield 96%). ^1H NMR (400 MHz, $CDCl_3$): δ 9.84 (s, 1H), 7.64 (d, J = 4.0 Hz, 1H), 7.17 (dd, J_1 = 3.6 Hz, J_2 = 3.6 Hz, 2H), 6.74 (d, J = 3.6 Hz, 1H), 2.81 (t, J = 7.6 Hz, 2H), 1.69 (m, 2H), 1.35 (m, 6H), 0.89 (t, J = 6.8 Hz, 3H).

Synthesis of Compound ***2***. 2,4-Dimethylpyrrole (1.6 mL, 15.5 mmol) and 2-thiophenecarboxaldehyde (841 mg, 7.5 mmol) were placed in a dry two-neck round bottle flask with 200 mL of CH_2Cl_2 inside. N_2 was purged for 1 h. Afterward, a small amount of trifluoroacetic acid was added in order to initiate the reaction. After 5 h, 2,3-dichloro-5,6-dicyano-1,4-benzoquinone (1.70 g, 7.5 mmol) was added at once. One hour later, $(i\text{-Pr})_2EtN$ (15 mL) was added to the purple reaction mixture followed by $BF_3{\cdot}Et_2O$ (15 mL) immediately. The reaction was quenched by adding 100 mL of water after 1 h. The mixture was extracted three times with CH_2Cl_2, and the organic phase was collected and evaporated under vacuum. Finally, the crude product was purified by column chromatography (eluent CH_2Cl_2/petroleum = 1/3) to give a red solid as the desired product (867 mg, yield 35%). ^1H NMR (300 MHz, $CDCl_3$): δ 7.50 (d, J = 5.1 Hz, 1H), 7.13 (t, J_1 = 3.3 Hz, J_2 = 5.1 Hz, 1H), 6.99 (d, J = 2.4 Hz, 1H), 6.00 (s, 2H), 2.55 (s, 6H), 1.58 (s, 6H).

Synthesis of Compound ***3***. The procedure is similar to synthesis of compound **2**, except that 5-bromothiophene-2-carboxaldehyde (1.43 g, 7.5 mmol) was used instead of 2-thiophenecarboxaldehyde. After the crude product was purified, a red solid (900 mg, yield 36%) was collected. ^1H NMR (300 MHz, $CDCl_3$): δ 7.10 (d, J = 3.6 Hz, 1H), 6.77 (d, J = 3.9 Hz, 1H), 6.02 (s, 2H), 2.55 (s, 6H), 1.70 (s, 6H).

*Synthesis of **H-T-BO***. A dry Schlenk tube was charged with compound **1** (317.0 mg, 0.96 mmol), compound **2** (552.0 mg, 2.00 mmol), and 30 mL of toluene. Afterward, the tube was purged with N_2 for 30 min. Then a small amount of molecule sieves was added followed by 1 mL of piperidine and 1 mL of CH_3COOH. The mixture was heated at 80 °C overnight. After cooling, the green mixture was poured into 50 mL of water and extracted three times with CH_2Cl_2, and the organic phase was collected and evaporated under vacuum. The residue was purified by column chromatography (eluent CH_2Cl_2/petroleum = 2/5). Recrystallization from EtOH can afford **H-T-BO** as a purple powder (326.0 mg, 40%). ^{1}H NMR (400 MHz, $CDCl_3$): δ 7.51 (d, J = 5.2 Hz, 1H), 7.50 (d, J = 16.0 Hz, 2H), 7.31 (d, J = 16.0 Hz, 2H), 7.10−7.15 (m, 5H), 7.05−7.02 (m, 3H), 6.72 (d, J = 3.6 Hz, 2H), 6.62 (s, 2H), 2.82 (t, J = 7.6 Hz, 4H), 1.69 (m, 4H), 1.64 (s, 6H), 1.26−1.42 (m, 12H), 0.90 (t, J = 7.6 Hz, 6H). ^{13}C NMR (100 MHz, $CDCl_3$): δ 152.15, 146.44, 141.81, 140.61, 140.01, 135.12, 134.83, 134.68, 129.73, 129.15, 129.04, 128.38, 127.55, 127.46, 125.15, 124.27, 123.80, 118.22, 117.97, 31.59, 31.57, 30.29, 28.79, 22.61, 14.13, 13.76. MS (MALDI-TOF): calcd for $C_{47}H_{49}BF_2N_2S_5$, 850.26; found m/z 850.5 (M^+). Anal. Calcd for $C_{47}H_{49}BF_2N_2S_5$: C, 66.33; H, 5.80; N, 3.29. Found: C, 66.55; H, 5.86; N, 3.25.

*Synthesis of **Br-T-BO***. The procedure is similar to that of **H-T-BO**, except compound **3** (393.2 mg, 0.96 mmol) was used instead of compound **2**. After being purified, a dark green crystal was afforded (339.8 mg, 38%). ^{1}H NMR (400 MHz, $CDCl_3$): δ 7.43 (d, J = 15.6 Hz, 2H), 7.32 (d, J = 15.6 Hz, 2H), 7.05−7.14 (m, 7H), 6.81 (d, J = 3.6 Hz, 1H), 6.72 (d, J = 3.6 Hz, 2H), 6.63 (s, 2H), 2.82 (t, J = 7.6 Hz, 4H), 1.75 (s, 6H), 1.66−1.74 (m, 4H), 1.25−1.42 (m, 12H), 0.90 (t, J = 6.8 Hz, 6H). ^{13}C NMR (100 MHz, $CDCl_3$): δ 152.44, 148.26, 146.55, 141.53, 140.54, 140.23, 136.93, 134.64, 130.30, 129.94, 129.38, 128.98, 125.17, 124.33, 123.84, 118.45, 117.82, 116.01, 113.78, 31.59, 31.56, 30.29, 28.78, 22.60, 14.12, 14.10. MS (MALDI-TOF): calcd for $C_{47}H_{48}BBrF_2N_2S_5$ 930.16; found m/z 930.7 (M^+). Anal. Calcd for $C_{47}H_{48}BBrF_2N_2S_5$: C, 60.70; H, 5.20; N, 3.01. Found: C, 60.95; H, 5.18; N, 3.02.

*Synthesis of **DIMER***. **Br-T-BO** (200 mg, 0.21 mmol), 2,5-bis(tributylstannyl)thiophene (63.0 mg, 0.095 mmol), and 15 mL of anhydrous toluene were added into a dry Schlenk tube. After being purged with argon for 30 min, $Pd(PPh_3)_4$ (20 mg, 0.017 mmol) was charged. Then the mixture was heated at 110 °C overnight. After cooling to room temperature, the mixture was poured into water and extracted with CH_2Cl_2 three times. The organic phase was collected and washed with brine and water and then dried over Na_2SO_4. The residue was then loaded on a silica gel column (eluent CH_2Cl_2/petroleum = 1/1) to produce **DIMER** as a black powder (67.8 mg, 40%). ^{1}H NMR (400 MHz, $CDCl_3$): δ 7.53 (d, J = 16.0 Hz, 4H), 7.33 (d, J = 16.0 Hz, 4H, overlapped with $CDCl_3$), 7.24 (d, J = 3.6 Hz, 2H, overlapped with $CDCl_3$), 7.05−7.17 (m, 14H), 6.95 (d, J = 3.6 Hz, 2H), 6.73 (d, J = 3.6 Hz, 4H), 6.65 (s, 4H), 2.82 (t, J = 8 Hz, 8H), 1.84−1.81 (d, 12H), 1.67−1.74 (m, 8H), 1.26−1.41 (m, 24H), 0.91 (t, J = 6.4 Hz, 12H). ^{13}C NMR (100 MHz, $CDCl_3$): δ 152.46, 146.64, 141.75, 140.71, 140.28, 139.21, 136.02, 134.93, 134.90, 134.79, 134.37, 130.03, 129.55, 129.40, 128.01, 125.30, 125.09, 124.44, 123.96, 118.50, 118.04, 31.72, 31.70, 30.42, 28.92, 22.74, 14.28, 14.26. MS (MALDI-TOF): calcd for $C_{98}H_{98}B_2F_4N_4S_{11}$ 1781.49; found m/z 1781.9 (M^+). Anal. Calcd for $C_{98}H_{98}B_2F_4N_4S_{11}$: C, 66.05; H, 5.54; N, 3.14. Found: C, 65.72; H, 5.58; N, 3.15.

■ ASSOCIATED CONTENT

Supporting Information

TGA curves, ^{1}H NMR spectra, ^{13}C NMR spectra, photovoltaic performance of the cell devices obtained under different conditions, out-of-plane and in-plane profiles, and XRD data. This material is available free of charge via the Internet at http://pubs.acs.org.

■ AUTHOR INFORMATION

Corresponding Author

*E-mail: clzhan@iccas.ac.cn.

Author Contributions

The manuscript was written through contributions of all authors. All authors have given approval to the final version of the manuscript.

Funding

National Natural Science Foundation of China (NSFC, Nos. 21327805, 91433202, 91227112, and 21221002), Chinese Academy of Sciences (CAS, XDB12010200), and Ministry of Science and Technology of the People's Republic of China (MOST, Project 973, 2011CB808400 and 2012YQ120060).

Notes

The authors declare no competing financial interest.

■ ACKNOWLEDGMENTS

We acknowledge the Beijing Synchrotron Radiation Facility (BSRF) for measurements of GIXRD and the assistance of the scientists there. We also acknowledge CAS for financial support.

■ REFERENCES

(1) Lu, L.; Yu, L. Understanding Low Bandgap Polymer PTB7 and Optimizing Polymer Solar Cells Based on It. *Adv. Mater.* **2014**, *26*, 4413−4430.

(2) Li, Y. Molecular Design of Photovoltaic Materials for Polymer Solar Cells: Toward Suitable Electronic Energy Levels and Broad Absorption. *Acc. Chem. Res.* **2012**, *45*, 723−733.

(3) Zhou, H.; Yang, L.; You, W. Rational Design of High Performance Conjugated Polymers for Organic Solar Cells. *Macromolecules* **2012**, *45*, 607−632.

(4) Chen, H. Y.; Hou, J.; Zhang, S.; Liang, Y.; Yang, G.; Yang, Y.; Yu, L.; Wu, Y.; Li, G. Polymer Solar Cells with Enhanced Open-Circuit Voltage and Efficiency. *Nat. Photonics* **2009**, *3*, 649−653.

(5) Guo, X.; Zhang, M.; Ma, W.; Ye, L.; Zhang, S.; Liu, S.; Ade, H.; Huang, F.; Hou, J. Enhanced Photovoltaic Performance by Modulating Surface Composition in Bulk Heterojunction Polymer Solar Cells Based on PBDTTT-C-T/$PC_{71}BM$. *Adv. Mater.* **2014**, *26*, 4043−4049.

(6) Li, X.; Choy, C. H.; Huo, L.; Xie, F.; Sha, W. E. I.; Ding, B.; Guo, X.; Li, Y.; Hou, J.; You, J.; Yang, Y. Dual Plasmonic Nanostructures for High Performance Inverted Organic Solar Cells. *Adv. Mater.* **2012**, *24*, 3046−3052.

(7) He, Z.; Zhong, C.; Su, S.; Xu, M.; Wu, H.; Cao, Y. Enhanced Power-Conversion Efficiency in Polymer Solar Cells Using an Inverted Device Structure. *Nat. Photonics* **2011**, *6*, 591−595.

(8) Chen, Y. S.; Wan, X. J.; Long, G. High Performance Photovoltaic Applications Using Solution-Processed Small Molecules. *Acc. Chem. Res.* **2013**, *46*, 2645−2655.

(9) Yu, Q. C.; Fu, W. F.; Wan, J. H.; Wu, X. F.; Shi, M. M.; Chen, H. Z. Evaluation of Heterocycle-Modified Pentathiophene-Based Molecular Donor Materials for Solar Cells. *ACS Appl. Mater. Interfaces* **2014**, *6*, 5798−5809.

(10) Tang, A.; Lu, Z.; Bai, S.; Huang, J.; Chen, Y.; Shi, Q.; Zhan, C.; Yao, J. Photocurrent Enhancement in Diketopyrrolopyrrole Solar Cells by Manipulating Dipolar Anchoring Terminals on Alkyl-Chain Spacers. *Chem.−Asian J.* **2014**, *9*, 883−892.

(11) Li, Z.; He, G.; Wan, X.; Liu, Y.; Zhou, J.; Long, G.; Zuo, Y.; Zhang, M.; Chen, Y. Solution Processable Rhodanine-Based Small Molecule Organic Photovoltaic Cells with a Power Conversion Efficiency of 6.1%. *Adv. Energy Mater.* **2012**, *2*, 74−77.

(12) Graham, K. R.; Mei, J.; Stalder, R.; Shim, J. W.; Cheun, H.; Steffy, F.; So, F.; Kippelen, B.; Reynolds, J. R. Polydimethylsiloxane as a Macromolecular Additive for Enhanced Performance of Molecular Bulk Heterojunction Organic Solar Cells. *ACS Appl. Mater. Interfaces* **2011**, *3*, 1210−1215.

(13) Zhou, J.; Wan, X.; Liu, Y.; Zuo, Y.; Li, Z.; He, G.; Long, G.; Ni, W.; Li, C.; Su, X.; Chen, Y. Small Molecules Based on Benzo[1,2-*b*:4,5-*b*′]dithiophene Unit for High-Performance Solution-Processed Organic Solar Cells. *J. Am. Chem. Soc.* **2012**, *134*, 16345−16351.
(14) van der Poll, T. S.; Love, J. A.; Nguyen, T.-Q.; Bazan, G. C. Non-Basic High-Performance Molecules for Solution-Processed Organic Solar Cells. *Adv. Mater.* **2012**, *24*, 3646−3649.
(15) Liu, X.; Sun, Y.; Hsu, B. B.; Lorbach, A.; Qi, L.; Heeger, A. J.; Bazan, G. C. Design and Properties of Intermediate-Sized Narrow Band-Gap Conjugated Molecules Relevant to Solution-Processed Organic Solar Cells. *J. Am. Chem. Soc.* **2014**, *136*, 5697−5708.
(16) Liu, J.; Walker, B.; Tamayo, A.; Zhang, Y.; Nguyen, T.-Q. Effects of Heteroatom Substitutions on the Crystal Structure, Film Formation, and Optoelectronic Properties of Diketopyrrolopyrrole-Based Materials. *Adv. Funct. Mater.* **2013**, *23*, 47−56.
(17) Dou, L.; You, J.; Hong, Z.; Xu, Z.; Li, G.; Street, R. A.; Yang, Y. 25th Anniversary Article: A Decade of Organic/Polymeric Photovoltaic Research. *Adv. Mater.* **2013**, *25*, 6642−6671.
(18) Wang, H.-Y.; Gao, J.; Gu, L.-J.; Wan, J.-H.; Wei, W.; Liu, F. Structural Modification of Thieno[3,4-c]pyrrole-4,6-dione: Structure−Property Relationships and Application in Solution-Processed Small-Molecule Organic Solar Cells. *J. Mater. Chem. A* **2013**, *1*, 5875−5885.
(19) Zhang, S.; Jiang, B.; Zhan, C.; Huang, J.; Zhang, X.; Jia, H.; Tang, A.; Chen, L.; Yao, J. Phenyl-1,3,5-Trithienyl-Diketopyrrolopyrrole: A Molecular Backbone Potentially Affording High Efficiency for Solution-Processed Small-Molecule Organic Solar Cells through Judicious Molecular Design. *Chem.−Asian J.* **2013**, *8*, 2407−2416.
(20) Feng, J.; Liang, B.; Wang, D.; Xue, L.; Li, X. Novel Fluorescent Dyes with Fused Perylene Tetracarboxlic Diimide and BODIPY Analogue Structures. *Org. Lett.* **2008**, *10*, 4437−4440.
(21) Zhu, S.; Zhang, J.; Vegesna, G.; Tiwari, A.; Luo, F.-T.; Zeller, M.; Luck, R.; Li, H.; Green, S.; Liu, H. Controlled Knoevenagel Reactions of Methyl Groups of 1,3,5,7-Tetramethyl BODIPY Dyes for Unique BODIPY Dyes. *RSC Adv.* **2012**, *2*, 404−407.
(22) Jiao, L.; Pang, W.; Zhou, J.; Wei, Y.; Mu, X.; Bai, G.; Hao, E. Regioselective Stepwise Bromination of Boron Dipyrromethene (BODIPY) Dyes. *J. Org. Chem.* **2011**, *76*, 9988−9996.
(23) Wu, W.; Guo, H.; Wu, W.; Ji, S.; Zhao, J. Organic Triplet Sensitizer Library Derived from a Single Chromophore (BODIPY) with Long-Lived Triplet Excited State for Triplet−Triplet Annihilation Based Upconversion. *J. Org. Chem.* **2011**, *76*, 7056−7064.
(24) Cakmak, Y.; Akkaya, E. U. Phenylethnyl-BODIPY Oligomers: Bright Dyes and Fluorescent Building Blocks. *Org. Lett.* **2009**, *11*, 85−88.
(25) Sekiya, M.; Umezawa, K.; Sato, A.; Citterio, D.; Suzuki, K. A Novel Luciferin-Based Bright Chemiluminescent for the Detection of Reactive Oxygen Species. *Chem. Commun. (Cambridge, U.K.)* **2009**, *45*, 3047−3049.
(26) Loudet, A.; Burgess, K. BODIPY Dyes and Their Derivatives Syntheses and Spectroscopic Properties. *Chem. Rev.* **2007**, *107*, 4891−4932.
(27) Wagner, R. W.; Lindsey, J. S. Boron-Dipyrromethene Dyes for Incorporation in Synthetic Multi-Pigment Light-Harvesting Arrays. *Pure Appl. Chem.* **1996**, *68*, 1373−1380.
(28) Lu, H.; Mack, J.; Yang, Y.; Shen, Z. Structural Modification Strategies for the Rational Design of Red/NIR Region BODIPYs. *Chem. Soc. Rev.* **2014**, *43*, 4778−4823.
(29) Lin, Y.; Li, Y.; Zhan, X. Small Molecule Semiconductors for High-Efficiency Organic Photovoltaics. *Chem. Soc. Rev.* **2012**, *41*, 4245−4272.
(30) Yoshii, R.; Yamane, H.; Nagai, A.; Tanaka, K.; Taka, H.; Kita, H.; Chujo, Y. π-Conjugated Polymers Composed of BODIPY or Aza-Bodipy Derivatives Exhibiting High Electron Mobility and Low Threshold Voltage in Electron-Only Devices. *Macromolecules* **2014**, *47*, 2316−2323.
(31) Usta, H.; Yilmaz, M. D.; Avestro, A. J.; Boudinet, D.; Denti, M.; Zhao, W.; Stoddart, J. F.; Facchetti, A. BODIPY−Thiophene Copolymers as *p*-Channel Semiconductors for Organic Thin-Film Transistors. *Adv. Mater.* **2013**, *25*, 4327−4334.
(32) He, W.; Jiang, Y.; Qin, Y. Synthesis and Photovoltaic Properties of a Low Bandgap BODIPY−Pt Conjugated Polymer. *Polym. Chem.* **2014**, *5*, 1298−1304.
(33) Bessette, A.; Hanan, G. S. Design, Synthesis and Photophysical Studies of Dipyrromethene-Based Materials: Insights into Their Applications in Organic Photovoltaic Devices. *Chem. Soc. Rev.* **2014**, *43*, 3342−3405.
(34) Cortizo-Lacalle, D.; Howells, C. T.; Gambino, S.; Vilela, F.; Vobecka, Z.; Findlay, N. J.; Inigo, A. R.; Thomson, S. A. J.; Skabara, P. J.; Samuel, I. D. W. BODIPY-Based Conjugated Polymers for Broadband Light Sensing and Harvesting Applications. *J. Mater. Chem.* **2012**, *22*, 14119−14126.
(35) Bura, T.; Leclerc, N.; Fall, S.; Lévêque, P.; Heiser, T.; Retailleau, P.; Rihn, S.; Mirloup, A.; Ziessel, R. High-Performance Solution-Processed Solar Cells and Ambipolar Behavior in Organic Field-Effect Transistors with Thienyl-BODIPY Scaffoldings. *J. Am. Chem. Soc.* **2012**, *134*, 17404−17407.
(36) Bura, T.; Leclerc, N.; Fall, S.; Lévêque, P.; Heiser, T.; Ziessel, R. Absorption Tuning of Monosubstituted Triazatruxenes for Bulk Heterojunction Solar Cells. *Org. Lett.* **2011**, *13*, 6030−6033.
(37) Rousseau, T.; Cravino, A.; Bura, T.; Ulrich, G.; Ziessel, R.; Roncali, J. BODIPY Derivatives as Donor Materials for Bulk Heterojunction Solar Cells. *Chem. Commun. (Cambridge, U.K.)* **2009**, *45*, 1673−1675.
(38) Qin, H.; Li, L.; Guo, F.; Su, S.; Peng, J.; Cao, Y.; Peng, X. Solution-Processed Bulk Heterojunction Solar Cells Based on a Porphyrin Small Molecule with 7% Power Conversion Efficiency. *Energy Environ. Sci.* **2014**, *7*, 1397−1401.
(39) Qin, T.; Zajaczkowski, W.; Pisula, W.; Baumgarten, M.; Chen, M.; Gao, M.; Wilson, G.; Easton, C. D.; Müllen, K.; Watkins, S. E. Tailored Donor−Acceptor Polymers with an A−D1−A−D2 Structure: Controlling Intermolecular Interactions to Enable Enhanced Polymer Photovoltaic Devices. *J. Am. Chem. Soc.* **2014**, *136*, 6049−6055.
(40) Huang, J.; Wang, X.; Zhang, X.; Niu, Z.; Lu, Z.; Jiang, B.; Sun, Y.; Zhan, C.; Yao, J. Additive-Assisted Control over Phase-Separated Nanostructures by Manipulating Alkylthienyl Position at Donor Backbone for Solution-Processed, Non-Fullerene, All-Small-Molecule Solar Cells. *ACS Appl. Mater. Interfaces* **2014**, *6*, 3853−3862.
(41) Huang, J.; Zhao, Y.; Ding, X.; Jia, H.; Jiang, B.; Zhang, Z.; Zhan, C.; He, S.; Pei, Q.; Li, Y.; Liu, Y.; Yao, J. Synthesis and Charge-Transporting Properties of Electron-Deficient CN2-Fluorene Based D-A Copolymers. *Polym. Chem.* **2012**, *3*, 2170−2177.
(42) Mishra, A.; Bäuerle, P. Small Molecule Organic Semiconductors on the Move: Promises for Future Solar Energy Technology. *Angew. Chem., Int. Ed.* **2012**, *51*, 2020−2067.
(43) Koster, L. J. A.; Mihailetchi, V. D.; Blom, P. W. M. Ultimate Efficiency of Polymer/Fullerene Bulk Heterojunction Solar Cells. *Appl. Phys. Lett.* **2006**, *88*, 093511.
(44) Scharber, M. C.; Mühlbacher, D.; Koppe, M.; Denk, P.; Waldauf, C.; Heeger, A. J.; Brabec, C. J. Design Rules for Donors in Bulk-Heterojunction Solar Cells—Towards 10% Energy-Conversion Efficiency. *Adv. Mater.* **2006**, *18*, 789−794.
(45) Sharma, G. D.; Mikroyannidis, J. A.; Kurchania, R.; Thomas, K. R. J. Organic Bulk Heterojunction Solar Cells Based on Solution Processable Small Molecules (A−π−A) Featuring 2-(4-nitrophenyl) acrylonitrile Acceptors and Phthalimide-Based π-Linkers. *J. Mater. Chem.* **2012**, *22*, 13986−13995.
(46) O'Connor, B.; An, K. H.; Pipe, K. P.; Zhao, Y.; Shtein, M. Enhanced Optical Field Intensity Distribution in Organic Photovoltaic Devices Using External Coatings. *Appl. Phys. Lett.* **2006**, *89*, 233502.
(47) Jiang, B.; Zhang, X.; Zhan, C.; Lu, Z.; Huang, J.; Ding, X.; He, S.; Yao, J. Benzodithiophene Bridged Dimeric Perylene Diimide Amphiphiles as Efficient Solution-Processed Non-Fullerene Small Molecules. *Polym. Chem.* **2013**, *4*, 4631−4638.
(48) Chu, T.-Y.; Song, O.-K. Hole Mobility of *N*,*N*-bis(naphthalen-1-yl)-*N*,*N*-bis(phenyl) benzidine Investigated by Using Space-Charge-Limited Currents. *Appl. Phys. Lett.* **2007**, *90*, 203512.
(49) Halls, J. J. M.; Cornil, J.; Santos, D. A. d.; Silbey, R.; Hwang, D.-H.; Holmes, A. B.; Brédas, J. L.; Friend, R. H. Charge- and Energy-

Transfer Processes at Polymer/Polymer Interfaces: A Joint Experimental and Theoretical Study. *Phys. Rev. B* **1999**, *60*, 5721−5727.
(50) Tan, Z. A.; Zhang, W. Q.; Zhang, Z. G.; Qian, D. P.; Huang, Y.; Hou, J. H.; Li, Y. F. High-Performance Inverted Polymer Solar Cells with Solution-Processed Titanium Chelate as Electron-Collecting Layer on ITO Electrode. *Adv. Mater.* **2012**, *24*, 1476−1481.